Temperature-Dependent High-Speed Dynamics of Terahertz Quantum Cascade Lasers

Gary Agnew, *Member, IEEE*, Andrew Grier, Thomas Taimre, *Associate Member, IEEE*, Karl Bertling, *Member, IEEE*, Yah Leng Lim, *Member, IEEE*, Zoran Ikonić, Paul Dean, Alexander Valavanis, Paul Harrison, Dragan Indjin, and Aleksandar D. Rakić, *Senior Member, IEEE*

***Abstract*—Terahertz frequency quantum cascade lasers offer a potentially vast number of new applications. To better understand and apply these lasers, a device-specific modeling method was developed that realistically predicts optical output power under changing current drive and chip temperature. Model parameters are deduced from the self-consistent solution of a full set of rate equations, obtained from energy-balance Schrödinger–Poisson scattering transport calculations. The model is, thus, derived from first principles, based on the device structure, and is, therefore, not a generic or phenomenological model that merely imitates the expected device behavior. By fitting polynomials to data arrays representing the rate equation parameters, we are able to significantly condense the model, improving memory usage and computational efficiency.**

***Index Terms*—Quantum cascade laser, rate equation model, electro-optical dynamics, thermal roll-over, bandwidth, turn-on behavior, free space communication.**

I. Introduction

THE terahertz (THz) band of frequencies [1] has become increasingly accessible in recent years via emerging technologies for generating and detecting THz radiation. Amongst the many potential applications are broadband short-range communication [2]–[6], heterodyne detection of exogenous THz radiation, imaging, and material analysis [7]. The THz quantum cascade laser, first demonstrated in 2002 [8], is a compact yet powerful semiconductor source of coherent THz radiation. Current devices are able to operate at temperatures as high as 129 K in continuous wave (cw) [9] and 200 K in pulsed mode [10], and emitting peak pulsed optical powers of greater than 1 W [11].

Modeling the dynamic behavior of THz QCLs is vital for understanding the more complex behaviors of these devices and thus for the development of new applications—more so, considering that laboratory investigation of such behavior can be prohibitively expensive and experimentally challenging due to the extraordinarily short timescales on which some phenomena occur. Further, a growing class of THz QCL applications relies on the self-mixing effect [12]–[14], in which emissions from the device are reflected from a target back into the laser cavity, yielding information about the target [15]. Such retro-injected light (optical feedback) alters the device state and behavior, introducing a new dimension of complexity into device behavior [16]. In these applications, a realistic model is an indispensable research tool. It may be necessary to consider the effects of optical feedback even where it is undesirable, as failure to do so can lead to unexpected outcomes in behavior [17], [18].

The exemplar laser modeled in this paper is a bound-to-continuum (BTC) type QCL, a device that is particularly challenging to model and optimize due to the relatively large number of quantum-confined subbands in the active region (AR). Full rate equation (RE) models can be solved in order to extract dynamical information relating to all the intersubband transitions. Since the intersubband scattering processes are both temperature and electric field strength (voltage) dependent, it is necessary to determine these dependencies via first principles in order to properly model a device. However, full RE modeling is computationally intensive and therefore restricted to static solutions. Moreover, solving full REs self-consistently with optical and thermal models is computationally challenging.

Reduced rate equations (RREs), which employ a subset of parameters derived from the full RE model, offer a simple and practical means of predicting a device's dynamic behavior without the need to repeatedly solve the full set of REs self-consistently. In principle, slight changes in a QCL's electric field distribution due to dynamical behavior necessitate re-calculation of the full self-consistent RE solution. In practice, ignoring the effect of these slight changes in electric field distribution on RRE parameters leads to a second-order error in the RRE solution that is commonly considered insignificant. This makes it possible

Manuscript received October 1, 2016; revised December 5, 2016; accepted December 8, 2016. Date of publication December 21, 2016; date of current version March 9, 2017. This work was supported under the Australian Research Council's Discovery Projects funding scheme (DP 160 103910) and the Queensland Government's Advance Queensland programme. This work was also supported by the Engineering and Physical Sciences Research Council, U.K., under Grants EP/J017671/1 and EP/J002356/1 and DTG award, by the Royal Society under Wolfson Research Merit Awards WM110032 and WM150029, and by the European Cooperation in Science and Technology (Action BM1205).

G. Agnew, K. Bertling, Y. L. Lim, and A. D. Rakić are with the School of Information Technology and Electrical Engineering, The University of Queensland, Brisbane, QLD 4072, Australia (e-mail: gary.agnew@uqconnect.edu.au; bertling@itee.uq.edu.au; ylim@itee.uq.edu.au; rakic@itee.uq.edu.au).

A. Grier was with the School of Electronic and Electrical Engineering, University of Leeds, Leeds LS2 9JT, U.K. He is now with Seagate Technology, Dublin, Ireland (e-mail: el09a2g@leeds.ac.uk).

T. Taimre is with the School of Mathematics and Physics, The University of Queensland, Brisbane, QLD 4072, Australia (e-mail: t.taimre@uq.edu.au).

Z. Ikonić, P. Dean, A. Valavanis, and D. Indjin are with the School of Electronic and Electrical Engineering, University of Leeds, Leeds LS2 9JT, U.K (e-mail: z.ikonic@leeds.ac.uk; P.Dean@leeds.ac.uk; a.valavanis@leeds.ac.uk; d.indjin@leeds.ac.uk).

P. Harrison is with the Materials and Engineering Research Institute, Sheffield Hallam University, Sheffield S1 1WB, U.K (e-mail: p.harrison@shu.ac.uk).

Color versions of one or more of the figures in this paper are available online at http://ieeexplore.ieee.org.

Digital Object Identifier 10.1109/JSTQE.2016.2638539

to use RREs for both dynamic and static modeling [19], and self-consistent computation of the emitted THz optical power.

However, a commonly made assumption in the use of the three-level RRE model for QCLs is that RRE parameters have constant values. All the RRE parameters are in fact both temperature- and voltage-dependent. Simulation results based on the assumption are therefore valid only over the narrow range of voltages and temperatures for which the RRE parameters were calculated.

Various approaches have been taken in dealing with this problem [19]–[22], usually by addressing either temperature-dependent or voltage-dependent device behavior in isolation. Our modeling approach, introduced in [23], overcomes this difficulty by accommodating the temperature- and voltage-dependence of all RRE parameters over the full operating range of the device. With the addition of an AR temperature model to our rate equations, we are able to predict lattice temperature under changing excitation and cold finger temperature, thereby accounting for the temperature-dependence of the RRE parameters. The resulting model is able to correctly reproduce the experimentally observed variations in emitted optical power, from the temperature-dependent threshold current, through roll-over to cut-off.

The aim of this paper is to both present our study of the dynamic turn-on behavior of a BTC THz QCL, and to provide a condensed version of our model to enable further investigation. In the following sections we define the model (Section II), setting out the complete generic model and providing device-specific data for a real (exemplar) QCL; discuss the results (Section III) of exemplar model applications to (A) static conditions, to simulate and explore its light–current (LI) characteristics and (B) turn-on behavior to characterize its high speed dynamics; and offer our concluding remarks.

II. Model Definition

A. Exemplar QCL

The QCL we chose to model is a single mode GaAs/AlGaAs BTC 2.59 THz device that has been processed into a surface-plasmon Fabry-Pérot ridge waveguide and operates up to temperatures of 50 K in cw. This device has been previously characterized and used in a variety of applications including material analysis [15], [24] and imaging [25]. The band structure is shown in Fig. 1, with the radiative transition's states labeled ULL and LLL. A complete specification of the active region heterostructure [26] is required to calculate device-specific RRE parameters from first principles.

B. Rate Equation Model

Our set of RREs reads:

$$\frac{\mathrm{d}S(t)}{\mathrm{d}t} = -\frac{1}{\tau_\mathrm{p}}S(t) + \frac{\beta_\mathrm{sp}}{\tau_\mathrm{sp}(T,V)}N_3(t) + MG(T,V)\frac{(N_3(t)-N_2(t))}{1+\varepsilon S(t)}S(t) \quad (1)$$

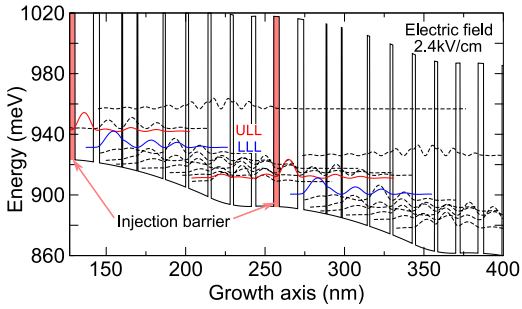

(a)

Fig. 1. Band diagram of our exemplar 2.59 THz BTC QCL. The radiative inter-subband transition is ULL → LLL (color online).

$$\frac{\mathrm{d}N_3(t)}{\mathrm{d}t} = -G(T,V)\frac{(N_3(t)-N_2(t))}{1+\varepsilon S(t)}S(t) - \frac{1}{\tau_3(T,V)}N_3(t) + \frac{\eta_3(T,V)}{q}I(t) \quad (2)$$

$$\frac{\mathrm{d}N_2(t)}{\mathrm{d}t} = +G(T,V)\frac{(N_3(t)-N_2(t))}{1+\varepsilon S(t)}S(t) + \frac{1}{\tau_{32}(T,V)}N_3(t) + \frac{\eta_2(T,V)}{q}I(t) - \frac{1}{\tau_{21}(T,V)}N_2(t) \quad (3)$$

$$\frac{\mathrm{d}T(t)}{\mathrm{d}t} = \frac{1}{mc_p}\left(I(t)V(T(t),I(t)) - \frac{(T(t)-T_0)}{R_\mathrm{th}}\right) \quad (4)$$

The symbol $S(t)$ represents photon population, τ_p the photon lifetime in the cavity, $N_3(t)$ the ULL carrier number, $N_2(t)$ the LLL carrier number, $I(t)$ the current forcing function, q the electronic charge, β_sp the spontaneous emission factor, τ_sp the spontaneous emission lifetime (or radiative spontaneous relaxation time), and M is the number of periods in the structure, 90 in the case of our exemplar QCL. The η_3 term in Eq. (2) models carrier injection efficiency into the ULL and the η_2 term in Eq. (3) models carrier injection efficiency directly into the LLL. The carrier lifetime for non-radiative transitions from the ULL to LLL is τ_{32}, the total lifetime due to non-radiative transitions for the ULL carrier population is τ_3, and the lifetime for transitions from the LLL to the continuum is τ_{21}. The gain factor is represented by G, as defined in [19]. We make provision for gain compression by including the term in ε in Eqs. (1)–(3).

Parameters that depend on temperature (T) and voltage (V) are expressed as functions of V and T, (V,T) in the RREs. These include the gain factor G, injection efficiencies η_3 and η_2, and carrier lifetimes τ_3, τ_{32}, τ_{21}, and z_{32}, the dipole matrix element, which is used to calculate τ_sp. The voltage V and temperature T are themselves time-dependent, but for the sake of readability are not written explicitly as functions of time t in Eqs. (1)–(3).

A requirement of modeling temperature-dependent device behavior is knowledge of the active region (AR) temperature. Changes in AR temperature will occur due to both changes in cold finger temperature and thermal gradients resulting from

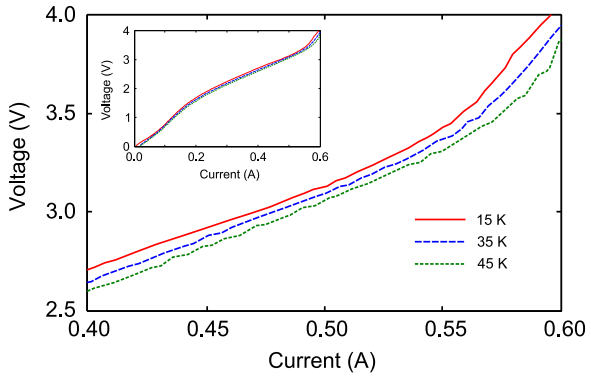

Fig. 2. Measured IV characteristics at $T_0 = 15$, 35 and 45 K. Inset: IV characteristics including current ranges over which the QCL does not lase. Polynomial coefficients of Eq. (12) for use in Eq. (4) were derived from the measured IV data set.

self-heating in cw operation. Further, any changes in excitation such as steps or ramps create thermal transients [27]–[29] that disturb the thermal circuit's equilibrium. Therefore in addition to three rate equations, a thermal model capable of predicting AR temperature must be included, and is represented by Eq. (4) in our equation set. This equation models the first order thermal behavior of the QCL and produces dynamic temperature response required to determine the temperature-sensitive RRE parameters at each step taken by the RRE solver. In Eq. (4), m represents the effective mass of the laser, c_p the effective specific heat capacity of the laser material in J kg^{-1} K^{-1} and $R_{\rm th}$ the effective thermal resistance in K W^{-1} between the AR and submount, which in this model is assumed to be at the same temperature as the cryostat's cold finger. The symbol T_0 is the temperature, in kelvin, of the cold finger which is usually (but not necessarily) constant.

Although the RREs are expressed in terms of a current forcing function $I(t)$, terminal voltage $V(t)$ is also required by the equations for two reasons: (i) calculation of self heating within the AR, as expressed in Eq. (4) and (ii) calculation of each of the ever-changing voltage-dependent RRE parameters. With $I(t)$ as the independent variable, $V(t)$ may be calculated from the temperature-dependent current–voltage (IV) characteristics of the QCL, shown in Fig. 2. This can be done via a behavioral (or other) model of $V(t)$ expressed in terms of $I(t)$ and $T(t)$. QCLs have IV characteristics somewhat different to, and more difficult to model theoretically, than those of diode lasers. For maximum accuracy we opted for a behavioral model based on measured temperature-dependent IV data, rather than use theoretically predicted IV characteristics.

Initial values for carrier and photon populations, the current forcing function $I(t)$, and T_0, serve as independent inputs to the RREs (1)–(4). Given these inputs, the RREs may be solved for carrier and photon populations. The optical output power $P(t)$ can then be found from the photon population by [20]:

$$P(t) = \eta_0 \hbar \omega S(t)/\tau_{\rm p}\,, \tag{5}$$

where η_0 is the power output coupling efficiency, $\hbar$ is the reduced Planck constant, and ω is the laser's angular emission frequency. The definition of η_0 is [20]:

$$\eta_0 = \frac{(1-R_1)\sqrt{R_2}}{(1-R_1)\sqrt{R_2}+(1-R_2)\sqrt{R_1}}\frac{\alpha_{\rm m}}{\alpha_{\rm m}+\alpha_{\rm w}}\,, \tag{6}$$

where R_1 is the front facet mirror reflectivity, R_2 the rear facet mirror reflectivity, $\alpha_{\rm w}$ the waveguide loss and $\alpha_{\rm m}$ the mirror loss defined as [21]:

$$\alpha_{\rm m} = \frac{-\ln(R_1 R_2)}{2L}\,, \tag{7}$$

where L is the length of the laser. We calculated the spontaneous emission lifetime $\tau_{\rm sp}$ from the dipole matrix element z_{32} using [21]:

$$\tau_{\rm sp} = \frac{\varepsilon_0 \hbar \lambda^3}{8\pi^2 q^2 n_{\rm eff} z_{32}^2}\,, \tag{8}$$

where λ is the wavelength of emission and $n_{\rm eff}$ the refractive index of the medium. The photon lifetime $\tau_{\rm p}$ is calculated from the modal loss via:

$$\tau_{\rm p} = \frac{n_{\rm eff}}{c(\alpha_{\rm w}+\alpha_{\rm m})} \tag{9}$$

Values for the various constants appearing in Eqs. (1)–(7) are given in Table I. Device-specific constants pertaining to our exemplar QCL are indicated by daggers in the table, and would need to be re-calculated for any new laser structure.

C. RRE Parameter Modeling

To determine the temperature- and voltage-dependent RRE parameters, a thermally-balanced self-consistent Schrödinger Poisson (SP) RE scattering transport model [30]–[32] for all states in the device was applied in a grid of 13 temperatures and 38 electric field (voltage) values. From these calculations we extracted values for the RRE parameters gain factor $G(T,V)$, ULL and LLL carrier lifetimes $\tau_3(T,V)$ and $\tau_{21}(T,V)$, injection efficiencies into these levels $\eta_3(T,V)$ and $\eta_2(T,V)$, the scattering time $\tau_{32}(T,V)$ between them, and the dipole matrix element $z_{32}(T,V)$ which is used in Eq. (8) for the calculation of $\tau_{\rm sp}(T,V)$. This yielded 494 (T,V) grid point values for each of the seven RRE parameters, giving 3458 data values in total.

A well-understood limitation of RE models of QCLs is the prediction of hybridized wave functions extending between periods of the QCL at certain biases [33], resulting in unrealistically large scattering rates being produced. All such non-physical parameters were identified and removed from the data set.

The plot of an example temperature- and voltage-dependent RRE parameter, η_3, is shown in Fig. 3.

Although each RRE parameter may be realized via interpolation as a function of T and V for use in Eqs. (1)–(4), the bulk of its data structure can be significantly reduced by polynomial fitting. The resulting polynomial coefficients can be viewed as a compressed form of the full RRE data, and polynomials present the additional benefit of de-noising and smoothing the bulk data—an important consideration in solving a set of stiff differential equations. The polynomial we chose for the purpose is a third order polynomial in V and T, fitted using a weighted

TABLE I
VALUE OF CONSTANTS USED IN EQS. (1)–(7)

Symbol	Value	Units	Meaning (†indicates device-specific)
$\tau_{\rm p}$	9.015	ps	†Photon lifetime in cavity
M	90	–	†Number of periods in QCL structure
$\beta_{\rm sp}$	1.627e-04	–	†Spontaneous emission factor
ε_0	8.854e-12	$\rm m^{-3}\,kg^{-1}\,s^4\,A^2$	Permittivity of free space
$\hbar$	1.055e-34	Js	Reduced Planck constant
λ	116	μm	†Wavelength of emission
ω	1.627e+13	rad $\rm s^{-1}$	†Angular frequency of emission
q	1.602e-19	C	Charge on the electron
$n_{\rm eff}$	3.30	–	†Effective refractive index of the medium
$R_{\rm th}$	8.2	$\rm KW^{-1}$	†Thermal resistance between active region and submount
m	1.533e-08	kg	†Mass of laser chip
$c_{\rm p}$	330	$\rm Jkg^{-1}\,K^{-1}$	†Effective specific heat capacity of laser chip
$\alpha_{\rm w}$	587.9	$\rm m^{-1}$	†Waveguide loss
R_1	0.324	–	†Front facet mirror reflectivity
R_2	0.324	–	†Rear facet mirror reflectivity
ε	0	–	†Gain compression factor
L	1.78	mm	†Length of laser chip cavity
c	3.00e08	$\rm m.s^{-1}$	Speed of light in a vacuum

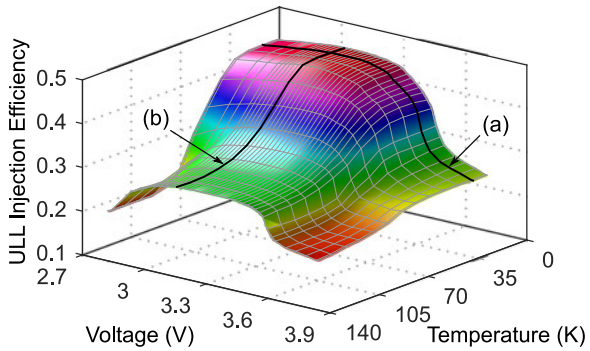

Fig. 3. Representation of η_3 as a surface, showing temperature and voltage dependence. Fall off in η_3 with increasing drive current occurs much more rapidly with voltage [trace (a)] than temperature [trace (b)], making it the primary cause of roll-over in this QCL.

least-squares method to give simple and smooth RRE parameter functions.

The general form of a polynomial in two independent variables is:

$$Z(x,y)=\sum_{i,j} a_{ij}x^i y^j\,, \tag{10}$$

where i and j are permuted subject to $(i+j)\le k$, and k is the order of the polynomial. The general third order polynomial expanded for variables T and V (in lieu of x and y) is:

$$Z(T,V)=a_{00}+a_{10}T+a_{01}V+a_{11}TV+a_{20}T^2+a_{02}V^2 +a_{21}T^2V+a_{12}TV^2+a_{30}T^3+a_{03}V^3 \tag{11}$$

Table II lists coefficient values for each of the temperature- and voltage-dependent RRE parameters found in (11). Terminal voltage $V(t)$ was modeled by fitting a third order polynomial of the following form to measured temperature-dependent current–voltage data:

$$V(I,T)=a_{00}+a_{10}I+a_{01}T+a_{11}IT+a_{20}I^2+a_{02}T^2 +a_{21}I^2T+a_{12}IT^2+a_{30}I^3+a_{03}T^3 \tag{12}$$

Coefficient values for this $V(t)$ model are also given in Table II.

D. Solution Process

The derivation of RRE parameters from full REs, fitting of polynomials to RRE data, and calculation of other structure-dependent items indicated in Table I, are a once-off process for each QCL structure. Once done, (1)–(4) may then be repeatedly solved for any chosen current excitation waveform and cold finger temperature. As with any ordinary differential equation (ODE) set, our equations, including the thermal model, have to be solved concurrently. While the solution is in progress, $V(t)$ is continuously re-calculated using Eq. (12) at every step the solver takes. The result is then fed into Eq. (4) to produce the time-dependent AR temperature $T(t)$. During this process $V(t)$ and $T(t)$ are simultaneously fed into the polynomial coefficients of all seven temperature- and voltage-dependent RRE parameters to update them. We used a well-known commercial ODE solver, Matlab's *ode23s* function, to produce the results following.

III. RESULTS AND DISCUSSION

A. Static Behavior

Characteristics that are easily measured in the laboratory, such as LI curves, are useful as a means of validating a model. We used the model to predict our exemplar QCL's LI characteristics by excitation with a slow current ramp $I(t)$ from 300 to 600 mA. The timescale of the ramp, 1 s, was far beyond that of the laser's electro-optic and thermal dynamics, giving a result that well represents the static response. The simulation was repeated for three cold finger temperatures, $T_0=15$ K,

TABLE II
POLYNOMIAL COEFFICIENT VALUES FOR MODELING VOLTAGE AND TEMPERATURE DEPENDENT RRE PARAMETERS

Coefficient	MG	η_3	η_2	τ_3	τ_{32}	τ_{21}	z_{32}	V
a_{00}	+2.5488e+04	+2.1969e-01	+6.7728e-03	+9.0220e-12	+1.9093e-10	+1.7446e-11	+6.0916e-09	−1.6880e-01
a_{10}	−5.3919e+02	+2.5332e-03	−1.1661e-04	+2.1018e-14	+1.8410e-12	+9.7705e-14	+1.8713e-11	+1.4024e+01
a_{01}	−4.1768e+04	−3.8617e+00	+1.9358e-02	+1.6585e-11	+4.7689e-10	−4.1352e-11	−8.4710e-09	−8.5203e-03
a_{11}	+2.7624e+02	−3.3045e-03	+8.5813e-05	−1.3866e-14	−7.5783e-13	+6.3343e-14	−1.4355e-11	−1.2368e-03
a_{20}	+5.6842e+00	−5.0512e-05	+1.2107e-06	−2.0161e-16	−3.9381e-14	−2.7574e-15	−3.4844e-13	−2.7018e+01
a_{02}	+2.1376e+04	+2.6028e+00	−1.3166e-02	−9.2287e-12	−2.7523e-10	+2.3966e-11	+5.2504e-09	+1.6206e-04
a_{21}	−1.8228e+00	+4.9878e-06	−6.7085e-07	+7.1827e-17	+5.6953e-15	−3.7009e-16	+5.7916e-14	+1.2415e-02
a_{12}	−3.0596e+01	+8.7604e-04	−1.4093e-05	+2.5180e-15	+1.2665e-13	−1.4482e-14	+3.1195e-12	−1.2573e-04
a_{30}	−1.4067e-02	+6.6497e-08	+1.8192e-08	−2.9601e-18	+4.2429e-17	+5.4384e-18	+3.4461e-16	+2.6099e+01
a_{03}	−2.8677e+03	−4.2682e-01	+2.1744e-03	+1.1832e-12	+3.7335e-11	−3.2744e-12	−7.8057e-10	−1.2635e-06

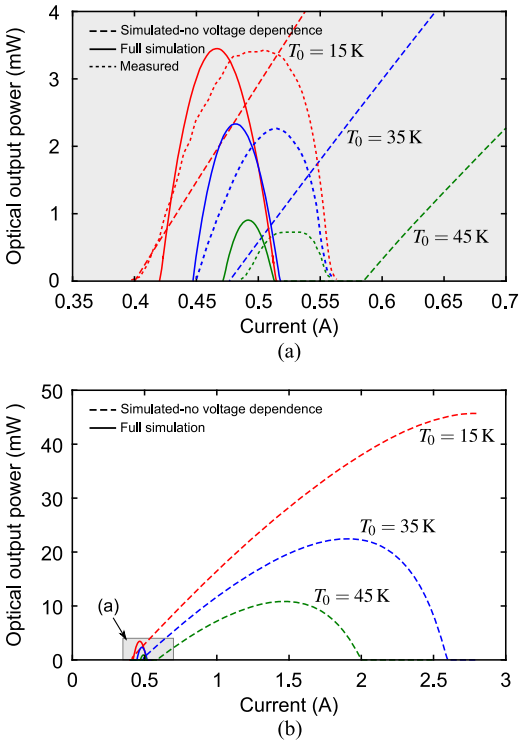

Fig. 4. Effect of RRE parameter voltage-dependence on LI characteristics. In part (a), solid lines are LI simulations *with* voltage dependent RRE parameters at $T_0 = 15$ K, 35 K and 45 K. Dotted lines are measured characteristics of the QCL at some of the same temperatures, vertically scaled by a factor of approximately four to compensate for the poor efficiency of the collection equipment. Dashed lines in parts (a) and (b) show LI simulations at the same temperatures, but with voltage-dependence of RRE parameters *suppressed* (parameters values locked at $V = 2.80$ V). Roll over observed in part (b) is thus thermal-only (i.e. due only to temperature-dependence of RRE parameters).

35 K, and 45 K, producing the results shown as solid curves in Fig. 4(a). Measured characteristics at some of the same cold finger temperatures, for comparison, are shown as dotted traces. The measured data were reduced in magnitude by a factor of approximately four due to the low collection efficiency of the detection optics. The data shown in Fig. 4(a) has been rescaled to match the simulated curves, for easy comparison. We are not aware of any other THz QCL model, to date, which is able to correctly predict roll-over behavior in QCLs.

As a demonstration of the part played by active region voltage in roll-over behavior, we repeated the simulation using RRE parameters that were temperature- but not voltage-dependent. This was done by assigning a constant value of $V = 2.80$ V in all RRE parameters, effectively making them voltage-independent. The results are shown as dashed lines in Fig. 4(a) and (b). Although threshold occurs at almost the same points as for the previous simulation, the LI curves are many times broader, with the resulting thermal-only roll-over occurring at far higher currents, demonstrating electric field effects to be the primary cause of roll-over in this type of device. Although the voltage-dependence of RRE parameters was suppressed in this simulation, $V(t)$ continued to be calculated via Eq. (12) for use in Eq. (4). We have previously reported the "full simulation" LI characteristics of this QCL [23], and reproduce them here for comparison with the hypothetical case of "non-voltage-dependent" RRE parameters.

The physical cause of voltage-related roll-over is a misalignment between the injector and ULL at higher voltages [34], that manifests as a rapid drop in injection efficiency η_3. Fig. 3 clearly shows that near roll-over η_3 drops far more rapidly due to voltage change (see trace (a) in Fig. 3) than due to temperature change [trace (b)].

B. Dynamic Behavior

The brief exploration here of our THz QCL's dynamic behavior aims to both illustrate the effects of temperature and voltage dependence on device behavior, and demonstrate the importance of modeling voltage-dependent device behavior. We chose to investigate basic dynamic behaviors that would be of interest in high speed applications, namely turn-on delay, rise time and overshoot in response to current-step excitation. Our first set of results, shown in Fig. 5, was obtained using an excitation current pulse of amplitude 0.470 A at the six cold finger temperatures indicated. Rise time τ_R and turn-on delay τ_D in the figure are as defined in [35]. Both turn-on delay and rise time are seen to increase non-linearly with increasing temperature, while the steady-state optical output power decreases and ceases altogether at ∼53 K. Because thermal effects take place on a microsecond scale, self-heating during the relatively short 4 ns pulse period may be ignored, making lattice and cold finger temperatures in this example effectively equal. The trend of rise time with temperature for 470 mA rectangular current pulses is shown in Fig. 6. We repeated the simulation to study rise time

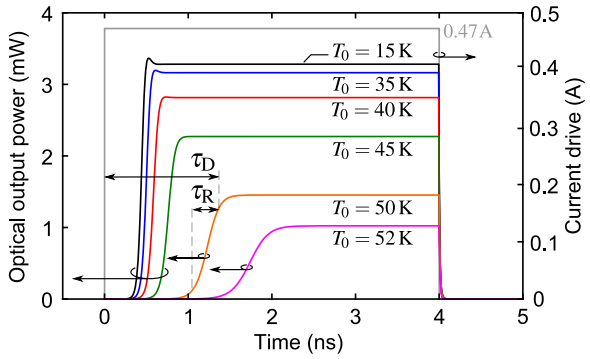

Fig. 5. Effect of cold finger temperature on step response. Response of the QCL to a current step of 0.470 A for six cold finger temperatures (color online) is shown, with both temperature- voltage-dependence of RRE parameters invoked. Both turn-on delay and pulse rise times increase with increasing cold finger temperature.

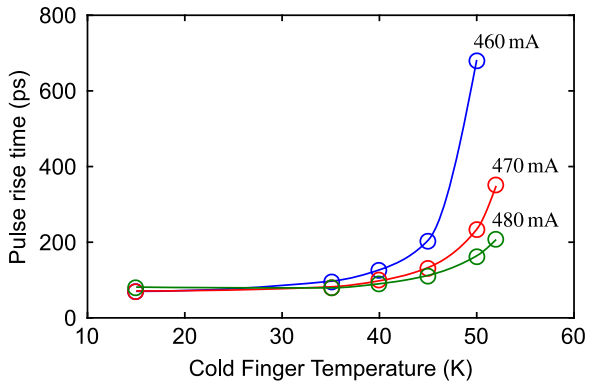

Fig. 6. Dependence of optical output power rise time on temperature for current step excitations of 460, 470, and 480 mA. Circles indicate data points, with curves to guide the eye.

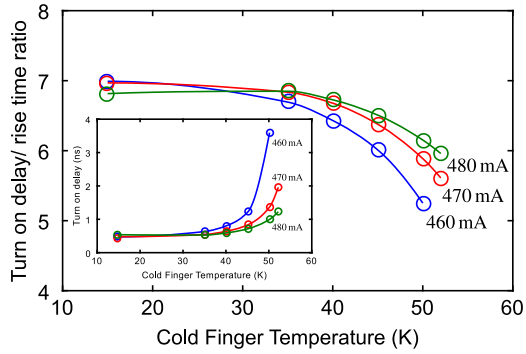

Fig. 7. Relation of turn-on delay and rise time. Inset: turn-on delay as a function of temperature for three currents. Circles indicate data points, with curves to guide the eye.

against temperature at pulse amplitudes of 460 mA and 480 mA (also shown in Fig. 6). In addition, turn-on delay was calculated for all simulations and is seen to correlate with rise time, as shown in Fig. 7. The sharp increase in both rise time (describing the speed of the system approaching saturation) and delay time (required for spontaneous emission to build up to a noticeable

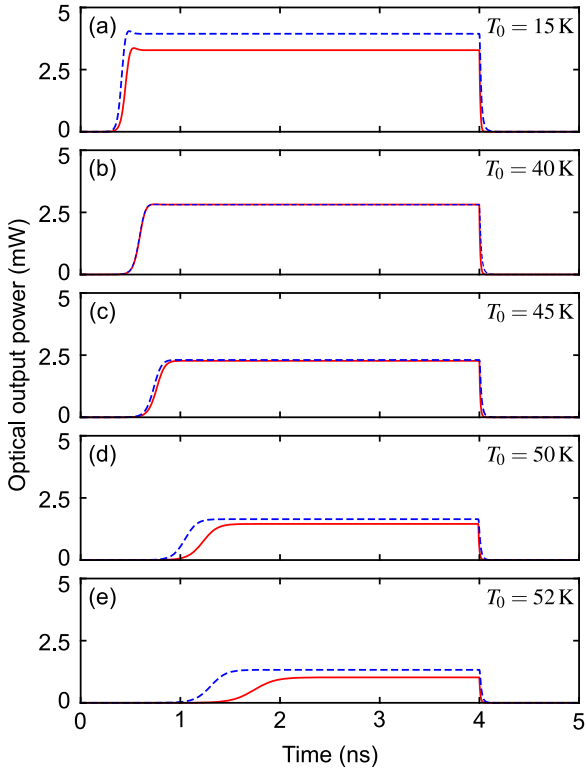

Fig. 8. Effect of cold finger temperature on 0.47 A step current response when voltage-dependence of RRE parameters is suppressed (values fixed for $V = 3.00$ V)—shown as dashed lines. For reference, solid lines (identical to those of Fig. 5) are responses with voltage-dependence invoked. Temperature- and voltage-dependence of RRE parameters is thus seen to have a significant effect on both turn-on delay and pulse rise time.

value), displayed in Fig. 6 and inset of Fig. 7, comes from the fast decrease of small-signal gain as the temperature increases. Their ratio does change somewhat with temperature (Fig. 7), but by a much smaller factor than they do individually. With the initial turn-on gain much larger than the saturated (or threshold) gain, one can expect that higher-order, more lossy modes will also temporarily exist before the laser stabilizes in the single mode of operation in steady state. However, this effect was not included in the present model.

To assess the impact of RRE parameter voltage-dependence on the behaviors shown in Fig. 5, we then repeated the simulation with voltage-dependence suppressed. This was done by assigning a constant voltage value $V = 3.00$ V in Eq. (11), the RRE polynomials. In other equations, i.e. Eqs. (12) and (4), use of temperature- and current-dependent voltage was retained. Non-voltage-dependent results are shown in Fig. 8 as dashed lines and, for comparison, voltage-dependent results as solid lines. The results demonstrate a significant difference when voltage is not taken into account, and agree only near the temperature at which the terminal voltage is actually 3.00 V.

We then explored the effect of different drive currents on turn-on dynamics, while holding the cold finger temperature constant at 15 K. Fig. 9 shows the results as solid lines for the five currents used. As before, we see a correlation between turn-on delay and rise time: starting with long times near threshold (part (a) of the

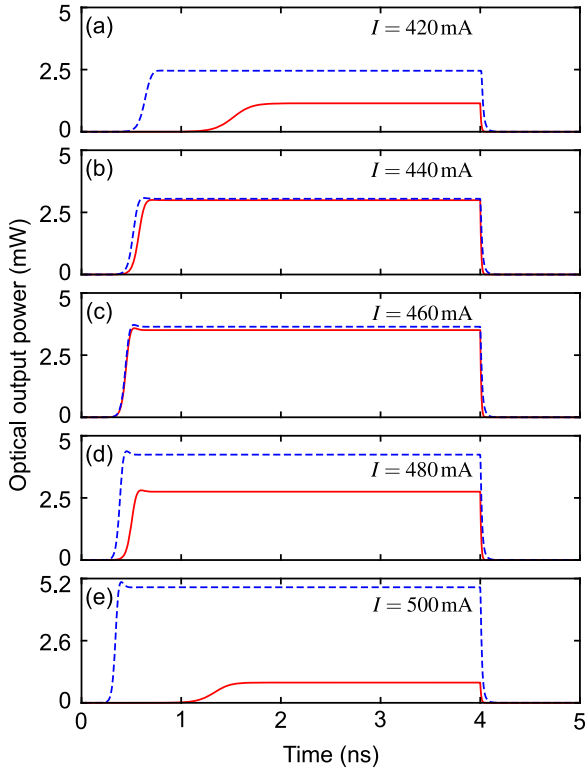

Fig. 9. Effect of RRE parameter voltage dependence on pulse response for constant cold finger temperature $T_0 = 15$ K and varying current drive. Parts (a)–(e) show QCL's response to five rectangular current pulses of amplitude 420, 440, 460, 480, and 500 mA. Solid lines represent the response with voltage-dependence of RRE parameters invoked and broken lines the response for voltage-dependence suppressed (for constant $V = 3.00$ V). Progressing from (a) to (e), peak optical power shown by the solid curves is seen to first rise and then fall, in accordance with the roll-over mechanism. For the broken curves it keeps rising due to the absence of the voltage-related roll-over mechanism.

figure), the times reduce to optimum values at about 460 mA and then lengthen again as injection efficiency η_3 rapidly falls off with increasing current. Optical power output follows the same trend, peaking at ∼460 mA and falling off rapidly just before cut-off (part(e) of the figure). When voltage-dependence of the RRE parameters is suppressed in the same way as before, however, response times continue shortening and optical power continues growing (broken lines in Fig. 9). Reduction in optical output power then peaks well after the known cut-off current of the QCL (not shown in figure), due to thermal-only effects, and in accordance with the LI characteristics of Fig. 4(b).

IV. Conclusion

We have presented a complete, computationally simple, dynamic model of an exemplar BTC THz QCL that behaves realistically over a wide range of voltages and temperatures. Our simulations reveal temperature- and bias-dependent turn-on characteristics that would be of interest in typically high speed free space communications and pulsed applications. They also demonstrate the importance of temperature- and voltage-dependence modeling, which has an impact on device behavior on timescales from pico-seconds to static. The novelty of our approach is the use of RRE parameters that are functions of device voltage and lattice temperature, derived from first principles by SP solution of the full set of REs. Coupled with a time dependent thermal equation, we obtain an RRE model that is valid over a broad range of device temperatures and voltages, allowing exploration of a QCL's characteristics over its full operating range of bias currents and temperatures. Although the RRE parameters presented here were derived for an exemplar BTC device, the approach is generic and may be applied to any QCL by extracting appropriate parameters from a full RE model.

References

[1] B. S. Williams, "Terahertz quantum-cascade lasers," *Nature Photon.*, vol. 1, pp. 517–525, 2007.
[2] R. Martini *et al.*, "Free-space optical transmission of multimedia satellite data streams using mid-infrared quantum cascade lasers," *Electron. Lett.*, vol. 38, no. 4, pp. 181–183, 2002.
[3] R. Martini and E. A. Whittaker, "Quantum cascade laser-based free space optical communications," *J. Opt. Fiber. Commun. Rep.*, vol. 2, no. 4, pp. 279–292, 2005.
[4] F. Capasso *et al.*, "Quantum cascade lasers: Ultrahigh-speed operation, optical wireless communication, narrow linewidth, and far-infrared emission," *IEEE J. Quantum Electron.*, vol. 38, no. 6, pp. 511–532, Jun. 2002.
[5] Z. Chen *et al.*, "Wireless communication demonstration at 4.1 THz using quantum cascade laser and quantum well photodetector," *Electron. Lett.*, vol. 47, no. 17, pp. 1002–1004, 2011.
[6] S. Barbieri *et al.*, "13 GHz direct modulation of terahertz quantum cascade lasers," *Appl. Phys. Lett.*, vol. 91, no. 14, 2007, Art. no. 143510.
[7] M. Tonouchi, "Cutting-edge terahertz technology," *Nature Photon.*, vol. 1, no. 2, pp. 97–105, 2007.
[8] R. Köhler *et al.*, "Terahertz semiconductor-heterostructure laser," *Nature*, vol. 417, no. 6885, pp. 156–159, 2002.
[9] M. Wienold *et al.*, "High-temperature, continuous-wave operation of terahertz quantum-cascade lasers with metal-metal waveguides and third-order distributed feedback," *Opt. Express*, vol. 22, no. 3, pp. 3334–3348, 2014.
[10] S. Fathololoumi *et al.*, "Terahertz quantum cascade lasers operating up to 200 k with optimized oscillator strength and improved injection tunneling," *Opt. Express*, vol. 20, no. 4, pp. 3866–3876, 2012.
[11] L. Li *et al.*, "Terahertz quantum cascade lasers with >1 W output powers," *Electron. Lett.*, vol. 50, no. 4, pp. 309–311, 2014.
[12] G. Giuliani, M. Norgia, S. Donati, and T. Bosch, "Laser diode self-mixing technique for sensing applications," *J. Opt. A: Pure Appl. Opt.*, vol. 4, no. 6, pp. 283–294, 2002.
[13] S. Donati, "Responsivity and noise of self-mixing photodetection schemes," *IEEE J. Quantum. Electron.*, vol. 47, no. 11, pp. 1428–433, Nov. 2011.
[14] T. Taimre *et al.*, "Laser feedback interferometry: A tutorial on the self-mixing effect for coherent sensing," *Adv. Opt. Photon.*, vol. 7, no. 3, pp. 570–631, 2015.
[15] A. D. Rakić *et al.*, "Swept-frequency feedback interferometry using terahertz frequency QCLs: A method for imaging and materials analysis," *Opt. Express*, vol. 21, no. 19, pp. 22194–22205, 2013.
[16] G. Agnew *et al.*, "Model for a pulsed terahertz quantum cascade laser under optical feedback," *Opt. Express*, vol. 24, no. 18, pp. 20554–20570, 2016.
[17] S. Donati and M. T. Fathi, "Transition from short-to-long cavity and from self-mixing to chaos in a delayed optical feedback laser," *IEEE J. Quantum Electron.*, vol. 48, no. 10, pp. 1352–1359, Oct. 2012.
[18] S. Donati and R. Horng, "The diagram of feedback regimes revisited," *IEEE J. Sel. Topics Quantum Electron.*, vol. 19, no. 4, Jul./Aug. 2012, Art. no. 1500309.
[19] Y. Petitjean, F. Destic, J. C. Mollier, and C. Sirtori, "Dynamic modeling of terahertz quantum cascade lasers," *IEEE J. Sel. Topics Quantum Electron.*, vol. 17, no. 1, pp. 22–29, Jan./Feb. 2011.
[20] A. Hamadou, J. L. Thobel, and S. Lamari, "Modelling of temperature effects on the characteristics of mid-infrared quantum cascade lasers," *Opt. Commun.*, vol. 281, no. 21, pp. 5385–5388, 2008.

[21] A. Hamadou, S. Lamari, and J. L. Thobel, "Dynamic modeling of a mid-infrared quantum cascade laser," *J. Appl. Phys.*, vol. 105, no. 9, 2009, Art. no. 093116.
[22] K. S. C. Yong, M. K. Haldar, and J. F. Webb, "An equivalent circuit for quantum cascade lasers," *J. Infrared Millimeter Terahertz Waves*, vol. 34, no. 10, pp. 586–597, 2013.
[23] G. Agnew *et al.*, "Efficient prediction of terahertz quantum cascade laser dynamics from steady-state simulations," *Appl. Phys. Lett.*, vol. 106, no. 16, 2015, Art. no. 161105.
[24] S. Han *et al.*, "Laser feedback interferometry as a tool for analysis of granular materials at terahertz frequencies: Towards imaging and identification of plastic explosives," *Sensors*, vol. 16, no. 352, pp. 1–9, 2016.
[25] Y. L. Lim *et al.*, "High-contrast coherent terahertz imaging of porcine tissue via swept-frequency feedback interferometry," *Biomed. Opt. Express*, vol. 5, no. 11, pp. 3981–3989, 2014.
[26] S. P. Khanna *et al.*, "The growth and measurement of terahertz quantum cascade lasers," *Phys. E*, vol. 40, no. 6, pp. 1859–1861, 2007.
[27] A. Valavanis *et al.*, "Time-resolved measurement of pulse-to-pulse heating effects in a terahertz quantum cascade laser using an NbN superconducting detector," *Appl. Phys. Lett.*, vol. 103, no. 6, 2013, Art. no. 061120.
[28] M. S. Vitiello, G. Scamarcio, and V. Spagnolo, "Time-resolved measurement of the local lattice temperature in terahertz quantum cascade lasers," *Appl. Phys. Lett.*, vol. 92, no. 10, 2008, Art. no. 101116.
[29] R. L. Tober, "Active region temperatures of quantum cascade lasers during pulsed excitation," *J. Appl. Phys.*, vol. 101, 2007, Art. no. 044507.
[30] P. Harrison and A. Valavanis, *Quantum Wells, Wires and Dots: Theoretical and Computational Physics of Semiconductor Nanostructures*, 4th ed. New York, NY, USA: Wiley, 2016.
[31] D. Indjin, P. Harrison, R. W. Kelsall, and Z. Ikonić, "Self-consistent scattering theory of transport and output characteristics of quantum cascade lasers," *J. Appl. Phys.*, vol. 91, no. 11, pp. 9019–9026, 2002.
[32] V. D. Jovanović *et al.*, "Influence of doping density on electron dynamics in GaAs/AlGaAs quantum cascade lasers," *J. Appl. Phys.*, vol. 99, no. 10, 2006, Art. no. 103106.
[33] H. Callebaut and Q. Hu, "Importance of coherence for electron transport in terahertz quantum cascade lasers," *J. Appl. Phys.*, vol. 98, no. 10, 2005, Art. no. 104505.
[34] S. S. Howard, Z. Liu, and C. F. Gmachl, "Thermal and stark-effect rollover of quantum-cascade lasers," *IEEE J. Quantum Electron.*, vol. 44, no. 4, pp. 319–323, Apr. 2008.
[35] K. Petermann, *Laser Diode Modulation and Noise*. Dordrecht, The Netherlands: Kluwer, 1991.

Gary Agnew (M'93) received the B.Sc. and M.Sc. degrees in electrical engineering from the University of the Witwatersrand, Johannesburg, South Africa, in 1985 and 1990, respectively. He is currently working toward the Ph.D. degree at the University of Queensland, Brisbane, Australia. He has held a number of research positions in the instrumentation industry, working on microwave, photonic, and nucleonic sensor technology. His research interests include modeling terahertz quantum cascade lasers.

Andrew Grier was born in Belfast, U.K. He received the B.Sc. (Hons.) degree in physics from the University of St. Andrews, St. Andrews, U.K., in 2009, and the M.Sc. and Ph.D. degrees in electronic and electrical engineering from the University of Leeds, Leeds, U.K., in 2010 and 2015, respectively. He is currently a Senior Research and Development Engineer at Seagate Technology, Dublin, Ireland. His research interests include computational modeling of carrier transport in semiconductor quantum electronics, and stochastic micromagnetic modeling of advanced magnetic recording devices.

Thomas Taimre received the B.Sc. degree in mathematics and statistics in 2003, the B.Sc. degree (with first honors) in statistics in 2004, and the Ph.D. degree in mathematics in 2009, all from the University of Queensland, Brisbane, Australia. He is a Lecturer of mathematics and statistics at the University of Queensland. He coauthored the book entitled *Handbook of Monte Carlo Methods*, which provides a hands-on guide to the theory, algorithms, techniques, and applications of Monte Carlo methods. His current research interests include the interface of probability theory, computer simulation, and mathematical optimization with biological and other scientific, engineering, and finance disciplines, including within laser feedback interferometry.

Karl Bertling (S'06–M'12) received the B.E. degree in electrical engineering and the B.Sc. degree in physics in 2003, the M.Phil. degree in electrical engineering in 2006, and the Ph.D. degree in electrical engineering in 2012, all from the University of Queensland, Brisbane, Australia. His current research interests include imaging and sensing via laser feedback interferometry (utilizing the self-mixing effect). He has contributed to the body of knowledge for this technique, in visible, near-IR, mid-IR, and terahertz semiconductor lasers.

Yah Leng Lim received the B.Eng. and Ph.D. degrees in electrical engineering from the University of Queensland, Brisbane, Australia, in 2001 and 2011, respectively. From 2002 to 2005, he was an R&D Engineer with the Philips Optical Storage (Singapore), where he worked on the integration of optical and sensor technologies in optical storage systems. He currently holds an Advance Queensland Research Fellowship funded by the Queensland Government, focusing on the development of laser feedback interferometry imaging systems for the early detection of skin cancers.

Zoran Ikonić received the Ph.D. degree in electrical engineering from the University of Belgrade, Belgrade, Serbia, in 1987. During 1981–1999, he was with the Faculty of Electrical Engineering, University of Belgrade. Since 1999, he has been with the School of Electronic and Electrical Engineering, University of Leeds, Leeds, U.K. His current research interests include electronic structure and optical and transport properties of semiconductor nanostructures and devices.

Paul Dean received the M.Phys. (Hons.) degree in physics and the Ph.D. degree in laser physics from the University of Manchester, Manchester, U.K., in 2001 and 2005, respectively. In 2005, he became a Postdoctoral Research Associate at the Institute of Microwaves and Photonics, School of Electronic and Electrical Engineering, University of Leeds, Leeds, U.K. In 2011, he received a Fellowship from the Engineering and Physical Sciences Research Council (U.K.). His current research interests include terahertz optoelectronics, quantum cascade lasers, and terahertz imaging techniques.

Alexander Valavanis received the M.Eng. (Hons.) degree in electronic engineering from the University of York, York, U.K., in 2004, and the Ph.D. degree in electronic and electrical engineering from the University of Leeds, Leeds, U.K., in 2009. From 2004 to 2005, he was an Instrumentation Engineer with STFC Daresbury Laboratories, Warrington, U.K., and from 2009 to 2016, he was a Research Fellow at the University of Leeds. He is currently a University Academic Fellow (tenure track) in terahertz instrumentation at the University of Leeds. His research interests include terahertz instrumentation, quantum cascade lasers, silicon photonics, and computational methods for quantum electronics. He is a member of the Institution of Engineering and Technology.

Paul Harrison is the Pro Vice-Chancellor for Research and Innovation at Sheffield Hallam University, Sheffield, U.K., where he also a member of the Materials and Engineering Research Institute. His research interests include the theoretical and computational physics of semiconductor nanostructures.

Dragan Indjin received the B.S., M.S., and Ph.D. degrees in electrical engineering from the University of Belgrade, Belgrade, Serbia.

He joined the Faculty of Electrical Engineering, University of Belgrade, in 1989, where he later became an Associate Professor. Since 2001, he has been with the Institute of Microwaves and Photonics, School of Electronic and Electrical Engineering, University of Leeds, Leeds, U.K., where he is a Reader (Associate Professor) in optoelectronics and nanoscale electronics. His research interests include the electronic structures, optical and transport properties, optimization and design of quantum wells, superlattices, quantum-cascade lasers, and quantum-well infrared photodetectors from near- to far-infrared and terahertz spectral ranges. He is currently focused on applications of quantum-cascade lasers and interband cascade lasers for sensing and imaging applications.

Dr. Indjin received the Prestigious Academic Fellowship from the Institute of Microwaves and Photonics, School of Electronic and Electrical Engineering, University of Leeds, in 2005. He is currently the coordinator of major international projects on infrared and terahertz imaging and sensing for medical and security application.

Aleksandar D. Rakić (M'93–SM'10) is a Professor with the School of Information Technology and Electrical Engineering, The University of Queensland, Brisbane, Australia, where he leads the Microwave, Photonics, and Communications group, focusing on the development of technologies for sensing and imaging across the electromagnetic spectrum including microwave, terahertz wave, and optical systems. Over the past ten years, his group has pioneered the development of several world's first laser-feedback interferometric sensors including systems based on monolithic vertical-cavity surface-emitting laser arrays (VCSELs), blue–green lasers, terahertz quantum cascade lasers, and mid-infrared interband cascade lasers. His current research interests include the development of sensing and imaging systems exploiting the terahertz spectrum for applications from security and defense to *in vivo* biomedical imaging. His other principal contributions are related to the design and characterization of surface-emitting optoelectronic devices (VCSELs and light-emitting diodes). He was an Invited Professor at the University of Toulouse during 2007–2012, and a Visiting Professor at the University of Leeds in 2012. He served as General Chair of the '2004 Conference on Optoelectronic and Microelectronic Materials and Devices, the co-Chair of the Symposium on Molecular and Organic Electronics and Organic Displays within the 2006 International Conference on Nanoscience and Nanotechnology, the Chair of the Symposium on Compound Semiconductor Materials and Devices within the 2008 International Conference on Electronic Materials, and the Chair of the IEEE AP/MTT Queensland Chapter.